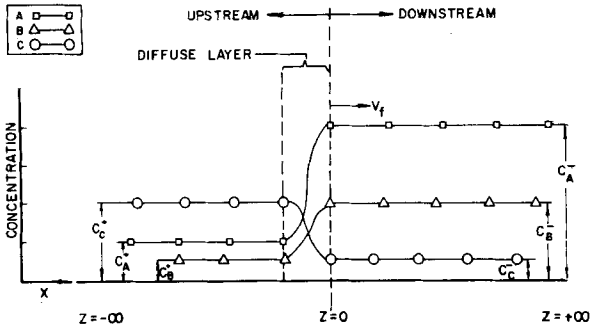

Figure 10. Corresponding aqueous phase concentrations as a function of position. The product of $C_A \cdot C_C$ equals the solubility product of $\overline{AC}$ everywhere even though $\overline{AC}$ is present only upstream.

where we have used Eqs. 17, 19 and 22. These equations may be integrated once to give

$$\frac{dC_A}{dz} = k_A e^{zD} + \frac{v_f}{K_l}(S_{\overline{AB}} - S_{\overline{AC}})e^{zD}H(z)$$

$$\frac{dC_B}{dz} = k_B e^{zD} - \frac{v_f}{K_l} S_{\overline{AB}} e^{zD}H(z)$$

$$\frac{dC_C}{dz} = k_C e^{zD} + \frac{v_f}{K_l} S_{\overline{AC}} e^{zD}H(z) \qquad (25)$$

where k_A, k_B and k_C are integration constants and $z_D = (v - v_f)$-z/K_l. A second integration yields

$$C_A = \frac{k_A K_l}{(v - v_f)} e^{zD} + \frac{v_f(S_{\overline{AB}} - S_{\overline{AC}})H(z)}{(v - v_f)}(e^{zD} - 1) + k'_A$$

$$C_B = \frac{k_B K_l}{(v - v_f)} e^{zD} - \frac{v_f S_{\overline{AB}} H(z)}{(v - v_f)}(e^{zD} - 1) + k'_B$$

$$C_C = \frac{k_C K_l}{(v - v_f)} e^{zD} + \frac{v_f S_{\overline{AC}} H(z)}{(v - v_f)}(e^{zD} - 1) + k'_C \qquad (26)$$

where k'_A, k'_B and k'_C are a second set of integration constants. We can combine constants and write out the Heaviside function explicitly to give

$$C_i = \begin{cases} k''_i e^{zD} + k'_i, & z < 0 \\ (k''_i + k'''_i)e^{zD} - k'''_i + k'_i, & z > 0 \end{cases} \qquad (27)$$

where

$$k''_i = \frac{k_i K_l}{(v - v_f)}, \quad i = A, B, C \qquad (28)$$

$$k'''_A = \frac{v_f(S_{\overline{AC}} - S_{\overline{AB}})}{(v - v_f)}$$

$$k'''_B = -\frac{v_f S_{\overline{AB}}}{(v - v_f)}$$

$$k'''_C = -\frac{v_f S_{\overline{AC}}}{v - v_f} \qquad (29)$$

We require a finite solution for z or z_D large; hence,

$$k''_i + k'''_i = 0, \quad i = A, B, C \qquad (30)$$

Furthermore, from the conditions at $z \to \pm\infty$ we gave

$$k'_i = C_i^+ \text{ and } k'_i - k'''_i = C_i^-, \quad i = A, B, C \qquad (31)$$

These conditions substituted into Eq. 33 give

$$C_i = \begin{cases} (C_i^- - C_i^+)e^{zD} + C_i^+, & z < 0 \\ C_i^-, & z > 0 \end{cases} \qquad (32)$$

Figure 10 shows the schematic profiles of Eq. 32. Now since $\overline{AC}$ is present for $z < 0$ we have

$$C_A C_C = K\frac{sp}{AC}, \quad z < 0 \qquad (33)$$

Substituting C_A and C_C into Eq. 33 from Eq. 32 and taking the limit as $z \to 0$ results in the downstream equilibrium condition, Eq. 20. Note that the C_i are constant for $z > 0$ but vary exponentially for $z < 0$. This means that a similar constraint does not apply on a region upstream of a dissolution wave as the reader may verify by applying the above procedure to the solid AB.

Fractionation with Condensation and Evaporation in Wetted-Wall Columns

A model is presented to describe the behavior of falling film fractionators with evaporation or condensation. Experimental measurements of vapor composition, vapor temperature and wall temperature profiles were made. Close agreement suggests that the model is applicable to both adiabatic and nonadiabatic conditions.

J. F. DAVIS, HSIEN-HSIN TUNG, and R. S. H. MAH

Department of Chemical Engineering
Northwestern University
Evanston, IL 60201

SCOPE

A distillation scheme which makes use of secondary reflux and vaporization (SRV) to enhance its thermal efficiency has shown considerable promise based on simulation results (Mah, et al., 1977; Fitzmorris and Mah, 1980). One promising physical realization of this scheme is to use a plate-fin device in which alternate and adjacent vertical channels serve as strippers and rectifiers (Mah, 1981). Because of heat transfer from the rectifying channels to the stripping channels, fractionation accompanied by condensation occurs continuously over the length of each rectifying channel. Similarly, fractionation accompanied by evaporation occurs over the length of each stripping channel. Unlike conventional distillation, the influence of a potentially large net mass flux between phases must be considered in modeling the SRV distillation scheme. Furthermore, because of the thermal coupling between the rectifier and

 J. F. Davis is now with the Department of Chemical Engineering, The Ohio State University. Correspondence concerning this paper should be addressed to R. S. H. Mah.

stripper, heat and mass transfer processes occurring in each are closely interrelated. It is critical that the design model should accurately predict temperature profiles as well as composition profiles.

A substantial literature has grown over the years on the modeling of simultaneous heat and mass transfer with large mass flux effects. In particular, condensation (Colburn and Drew, 1937; Sparrow and Marshall, 1969; Hoffman, 1971; Denny and Jusionis, 1972; Schrodt, 1973; Price and Bell, 1974; and Krishna and Panchal, 1977), evaporation (Shock, 1976; Watanabe and Munakata, 1976; Bergles et al., 1981), and gas absorption (Treybal, 1969; Stockar and Wilke, 1977a,b; Feintuch and Treybal, 1978) have been extensively studied. In the vapor phase, the film theory (Pratt and Tuohey, 1979; Krishna, 1981) is generally preferred because of its simplicity and comparable accuracy to boundary layer theory (Bird et al., 1960). For the liquid phase, either penetration theory or direct application of transport equations has been used.

In comparison with the theoretical development, surprisingly little published data are available for the purpose of model validation. Most of the published data have been obtained in fractionating condenser experiments. Generally the data consist of average values of inlet and outlet compositions and temperatures (Van Es and Heertjes, 1962; Onda et al., 1970; Ito and Asano, 1982). Kent and Pigford (1953, 1956) measured vapor composition profiles, but presented no data on vapor temperature profiles. No fractionating evaporator experiments were reported.

In this paper, we focus on the modeling of fractionating condensation and evaporation in wetted-wall columns as a first step towards a design procedure for SRV distillation using plate-fin devices. The ability of the model to predict not only composition profiles but also temperature profiles is emphasized. Vapor composition, vapor temperature and wall temperature profiles from fractionating condensation and evaporation experiments were used to select an appropriate mathematical model.

CONCLUSIONS AND SIGNIFICANCE

The columns were operated under total reflux conditions with a maximum vapor temperature difference of 30 K, a maximum vapor composition difference of 30 mol %, a maximum wall temperature difference of 10 K across the lengths of the columns. The maximum reboiler vapor flow rate was 6×10^{-5} kmol/s. With aluminum as the principal material of construction, the temperature drop across the wall was quite small, while axial heat conduction over the 2.32 m column length could be neglected in comparison with the enthalpy flows of the vapor and the liquid. The n-hexane-toluene mixture provides for a wide range of separation and temperatures, and a stable liquid film over these conditions. But it poses potential safety problems because of its toxicity and flammability, which required careful equipment design and selection. Closure on energy balances was found to average approximately 4% with the worst case at 13%.

Good agreement was obtained with a model based on the film theory in the vapor phase and zero mass transfer resistance and linear temperature profile in the liquid phase. Maximum deviations between the measurements and predictions were found to be 3 mol % in vapor composition, 6 K in vapor temperature, 2 K in wall temperature and 1.2×10^{-5} kmol/s in reboiler vapor flow rate. The best fit was obtained using: Eq. 11, a Nusselt-type equation, for the liquid heat transfer coefficient in condensation; and Eq. 23 from Chun and Seban (1973) for the same coefficient in evaporation. Comparison with Kent's data (1953) shows a maximum deviation of 6 mol % in vapor composition over a maximum operating range of 20 mol %.

Comparison was also made with a more elaborate model which attempts to account for mass transfer resistance and nonlinear temperature profile in the liquid phase. Numerical difficulties were encountered using this model. The agreement was generally quite poor even when comparison was possible.

On the basis of this study, we conclude that the proposed model gives prediction of fractionating condensation and evaporation in wetted-wall columns with an accuracy which is supported by the current experimental data.

SYSTEM DESCRIPTION

The system under investigation consists of a falling liquid film in laminar flow, which exchanges heat with its contiguous wall and which is countercurrent to an upward flow of vapor. To be quite specific, we shall consider the case of a binary mixture with heat input through the wall, as shown in Figure 1. A similar description will clearly apply to the case of heat removal through the wall.

Starting with the heat flux Q through the wall, the bulk of the heat transfer is in the transverse direction s. Heat is transferred through the falling film and the liquid-vapor interface into the vapor phase. A small fraction of the heat transferred through the wall is carried down by the falling film and contributes to the continuous increase in the liquid temperature as we move down the column.

At the liquid-vapor interface it is commonly assumed that the two phases are in thermodynamic equilibrium. Except at an azeotropic composition, the mole fraction of the more volatile component will be higher on the vapor side than on the liquid side. Relative to the liquid composition at the interface, the more volatile component will be transferred from the liquid phase to the vapor phase at a greater rate than the less volatile component. This relative transfer rate causes a local decrease of the concentration of the more volatile component and a build-up of the concentration

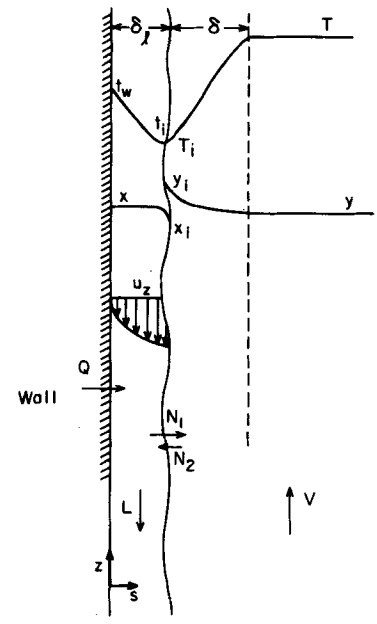

Figure 1. Temperature, concentration and velocity profiles in a falling liquid film and adjacent vapor phase.

gradient which is accompanied by mass diffusion. This description will hold true regardless of the direction of net mass transfer. However, the existence of wall heat input will superimpose a net evaporation on the aforementioned mass transfer process. The energy flux also induces a net mass flux across the interface.

The description on the vapor side is dominated by the turbulent flow regime. In the bulk vapor phase, both temperature and composition (in mole fraction) will be constant in the transverse direction. According to the film theory, nonzero vapor temperature and concentration gradients will be confined to a thin film adjacent to the vapor-liquid interface.

MATHEMATICAL MODEL

In the following derivation conduction and diffusion in the z direction are neglected, since they are usually small in comparison with convection. The sign of a variable is taken to be the same as that of s or z. With this sign convention the numerical values of L, N_2 and u_z are negative and those of V, N_1 and Q are positive in Figure 1, where L and V are the molar flow rates of vapor and liquid per unit length of wetted perimeter, N_1 and N_2 are the molar fluxes of component 1 and component 2 from the liquid phase to the vapor phase, and u_z is the liquid velocity in the vertical direction.

Consider a small section of the column from height z to $z + dz$. Applying mass balance to the vapor and the liquid volumes in turn, we have

$$\frac{dV}{dz} = N_1 + N_2 \tag{1}$$

$$\frac{dL}{dz} = -\frac{dV}{dz} \tag{2}$$

Similarly, if x and y are the mole fractions of the more volatile component in the liquid and the vapor phase, respectively, we have the following component material balances:

$$\frac{d(Vy)}{dz} = N_1 = K_G^{\bullet}(y_i - y) + y_i\frac{dV}{dz} \tag{3}$$

$$\frac{d(Lx)}{dz} = -\frac{d(Vy)}{dz} \tag{4}$$

where y_i is the vapor mole fraction of the more volatile component at the interface, $K_G^{\bullet}$ is the mass transfer coefficient in the vapor phase. The superscript "$\bullet$" indicates a transfer coefficient corrected for finite mass transfer rate through the interface.

The energy balances around the vapor and the liquid volumes may be obtained in an analogous manner taking into account the heat input through the column wall. These equations are given below:

$$\frac{d(V\mathcal{H})}{dz} = H_G^{\bullet}(T_i - T) + N_1\mathcal{H}_{1,i} + N_2\mathcal{H}_{2,i} \tag{5}$$

$$\frac{d(L\mathcal{h})}{dz} = -\frac{d(V\mathcal{H})}{dz} + Q \tag{6}$$

where $\mathcal{h}$ and $\mathcal{H}$ are molar enthalpies of the liquid and vapor averaged over the bulk flows, $\mathcal{H}_{1,i}$ and $\mathcal{H}_{2,i}$ are the partial vapor molar enthalpies of component 1 and component 2 at the interface, and $H_G^{\bullet}$ is the vapor phase film heat transfer coefficient.

Before we can solve these six differential equations for V, L, y, x, T and t, we need to compute N_1, N_2, $K_G^{\bullet}$, $H_G^{\bullet}$, y_i, T_i given the wall heat input Q. Procedures for calculating these parameters are developed in the next three sections.

Heat and Mass Transfer in the Liquid Phase

For falling films under laminar flow conditions Kotake and Oswatitsch (1980) obtained the following approximations which are derived in the appendix:

$$x = x_i \tag{7}$$

$$t = t_i + Q(\delta_l - s)/k_l \tag{8}$$

and

$$u_z = \rho_l s g(s - 2\delta_l)/(2\mu_l) \tag{9}$$

where δ_l is the thickness of the falling film, k_l, ρ_l and μ_l are the local liquid thermal conductivity, density and viscosity, and g is the gravitational acceleration. Equation 8 in this approximation replaces Eq. 6, both being derived from an energy balance around the falling liquid film.

We shall now define a liquid phase heat transfer coefficient, h_W, to relate the liquid temperatures at the wall and at the vapor-liquid interface:

$$Q = h_W(t_W - t_i) \tag{10}$$

Combining with Eq. 8, we have

$$h_W = k_l/\delta_l \tag{11}$$

where the falling film thickness δ_l is obtained by integration over s using Eq. 9:

$$\int_0^{\delta_l} \rho_l u_z ds = \frac{\rho_l^2 g}{2\mu_l}[s^3/3 - s^2\delta_l]_0^{\delta_l}$$

$$= -\frac{\rho_l^2 g \delta_l^3}{3\mu_l}$$

$$= LM_l$$

$$\delta_l = [3|L|M_l\mu_l/(g\rho_l^2)]^{1/3} \tag{12}$$

M_l is the average molecular weight of the liquid.

Heat and Mass Transfer in the Vapor Phase

For the vapor phase the mass transfer coefficient is given by Chilton and Colburn (1934),

$$K_G = 0.0228Re^{-0.17}Sc^{-2/3}W \tag{13}$$

where W is the vapor molar flux, Re is the Reynolds number defined in terms of the hydraulic diameter and Sc is the Schmidt number. Using the Chilton-Colburn analogy the heat transfer coefficient is given by

$$H_G = K_G Cp_v M_v (Sc/Pr)^{2/3} \tag{14}$$

where Cp_v is the bulk vapor heat capacity.

For finite mass flux through the liquid-vapor interface, the film theory has been applied to correct the heat and mass transfer coefficients (Bird et al., 1960). The corrected expressions are

$$K_G^{\bullet} = K_G\phi/(e^{\phi} - 1), \qquad \phi = (N_1 + N_2)/K_G \tag{15}$$

$$H_G^{\bullet} = H_G\psi/(e^{\psi} - 1), \qquad \psi = (N_1M_1Cp_1 + N_2M_2Cp_2)/H_G \tag{16}$$

where the heat capacities refer to the values at the interface. Equations 15 and 16 give the limiting values for zero mass flux, as ϕ and ψ go to zero.

Conditions at the Liquid-Vapor Interface

The following equations are imposed by phase equilibrium at the interface:

$$y_i = y_i(T_i, P) \tag{17}$$

$$x_i = x_i(t_i, P) \tag{18}$$

$$t_i = T_i \tag{19}$$

The equilibrium condition dictates that there be no temperature jump across the interface.

From Eq. 3 we obtain the component material balance across the interface,

$$N_1 = K_G^{\bullet}(y_i - y) + y_i(N_1 + N_2) \tag{20}$$

TABLE 1. CORRELATIONS AND MIXING RULES FOR ESTIMATION OF PHYSICAL PROPERTIES

Property	Liquid Phase	Vapor Phase
Vapor Pressure		
Pure Component	Reid et al., 1977, Eq. 6-3.1	
Mixture	Hirata et al., 1975, Chap. 1, Eqs. 23–30	
Latent Heat		
Pure Component	Reid et al., 1977, Eq. 6-16.1	
Mixture	$x \cdot \lambda_1 + (1 - x) \cdot \lambda_2$	
Heat Capacity		
Pure Component	Constant	Reid et al., 1977, Eq. 7-3.1
Mixture	$x \cdot Cp_{l,1} + (1 - x)Cp_{l,2}$	$y \cdot Cp_{v,1} + (1 - y)Cp_{v,2}$
Viscosity		
Pure Component	Perry and Chilton, 1973, Eq. 3-121	Reid et al., 1977, Eqs. 9-4.17 to 9-4.20
Mixture	Perry and Chilton, 1973, Eq. 3-122	Reid et al., 1977, Eq. 9-5.4
Diffusivity		
Mixture		Reid et al., 1977, Eq. 11-3.2
Thermal Conductivity		
Pure Component	Reid et al., 1977, Eq. 10-9.5	Reid et al., 1977, Eqs. 10-3.18 to 10-3.19
Mixture	Reid et al., 1977, Eq. 10-12.2	Perry and Chilton, 1973, Eq. 3-101
Density		
Pure Component	Perry and Chilton, 1973, Eq. 3-26a	Ideal Gas Behavior
Mixture	Additive Volume	same as above

Neglecting the effect of potential energy, kinetic energy, frictional losses and surface tension, we can also write the following energy balance across the interface:

$$-k_l \left.\frac{\partial t}{\partial s}\right|_{\delta_l} = H_G^*(T_i - T) + N_1\lambda_1 + N_2\lambda_2 \qquad (21)$$

which may be reexpressed using Eq. 8 as

$$Q = H_G^*(T_i - T) + N_1\lambda_1 + N_2\lambda_2 \qquad (22)$$

COMPUTING PROCEDURE

The model developed in the last section was used to compute conditions in the fractionating condensation and evaporation experiments. Because the top of the column was designed to minimize entrance effects the equations were integrated from the top in all cases. The initial conditions required were the temperatures, flow rates and mole fractions of the vapor and the liquid streams at the top of the column. In addition, the wall heat flux, column length, hydraulic diameter and pressure must also be specified.

The computation proceeds according to the following steps:

1. The physical properties of vapor and liquid stream were evaluated. The properties include vapor pressure, latent heat, heat capacity, viscosity, diffusivity, thermal conductivity and density. The methods used are given in Table 1.
2. Equations 13 and 14 were used to compute the transfer coefficients K_G, H_G.
3. Equations 7 and 18 were used to compute x_i and t_i which was subsequently used in Eqs. 19 and 17 to compute T_i and y_i.
4. Equations 20 and 22 were used to compute N_1 and N_2. These equations were solved iteratively along with Eqs. 15 and 16.
5. Equations 1–5 were integrated numerically to compute L, V, x, y and $\mathcal{H}$. The wall temperature t_w was computed using Eqs. 10–12.
6. The above steps were repeated in each step of numerical integration.

The equations were found to be numerically stable. The computing procedure worked satisfactorily with either Adams' or Euler's method.

COLUMN DESIGN AND OPERATING RANGE

Contrary to the general practice of using round-tube columns for wetted-wall experiments, a rectangular configuration was chosen in our experimentation. Such a configuration accommodates vapor composition, vapor temperature and wall temperature measurements along the length of the columns, which are difficult to obtain from round-tube columns when the column wall is either heated or cooled. In a rectangular geometry the liquid flows down one wall which can be heated or cooled while the vapor flows upward countercurrently. This arrangement permits easy access to the vapor phase with no interference of the liquid film. It leaves the outside surface of the wetted-wall free for heat input or removal. The other three walls along which the vapor flows are adiabatic and dry.

Since the heat and mass transfer coefficient correlations have been obtained from experiments in round-tube columns, an experimental check of the Chilton-Colburn gas phase mass transfer coefficient correlation (1937) using a hydraulic diameter was carried out. Measured and predicted HTU's (height of transfer units = $W/\{K_G a\}$) under adiabatic operation conditions were 1.08 and 1.18 m, respectively. The close agreement suggests that round and rectangular column results are compatible. Further confirmation of this compatibility through use of a hydraulic diameter may be found in the results of Hartnett et al. (1962).

Based on total reflux operation, the dimensions selected for the rectangular cross-section were 0.152 m × 0.00953 m. These dimensions were determined primarily to maximize the composition and temperature changes of the hexane-toluene system over a column height of 2.32 m while providing for a wide operating range. The column was designed to operate at a pressure which is only slightly above 1.013×10^5 Pa for ease of obtaining vapor samples. At this pressure flooding was estimated to occur at a vapor flow rate of 1.6×10^{-4} kmol/s (Clift et al., 1966).

No data were found to permit the onset of significant liquid entrainment to be estimated with confidence. Entrainment in cocurrent upward and downward annular flow was estimated to occur at flow rates of 1.3×10^{-4} kmol/s and 4.1×10^{-4} kmol/s, respectively (Hewitt and Hall-Taylor, 1970, pp. 136, 141). Since entrainment for a countercurrent flow situation would be expected to be at a lower value, the upper operating limit of the column was set conservatively at 9.0×10^{-5} kmol/s. Below this flow rate entrainment is expected to be negligible, since pressure drop and interfacial shear are negligible (Hewitt and Hall-Taylor, 1970, p. 70).

A conservative estimate of the minimum liquid flow rate for producing a stable liquid layer was calculated to be 3.4×10^{-5} kmol/s (Ponter et al., 1967). However, experimental measurements of the minimum flow rate showed that it could be no larger than 1.3×10^{-5} kmol/s. This is lower than the minimum turbulent vapor flow rate of 1.8×10^{-5} kmol/s (Hartnett et al., 1962). Since practical operating conditions will most likely be in the turbulent vapor flow regime, the minimum turbulent vapor flow rate was set as the lower operating limit. Thus, the effective operating range of the

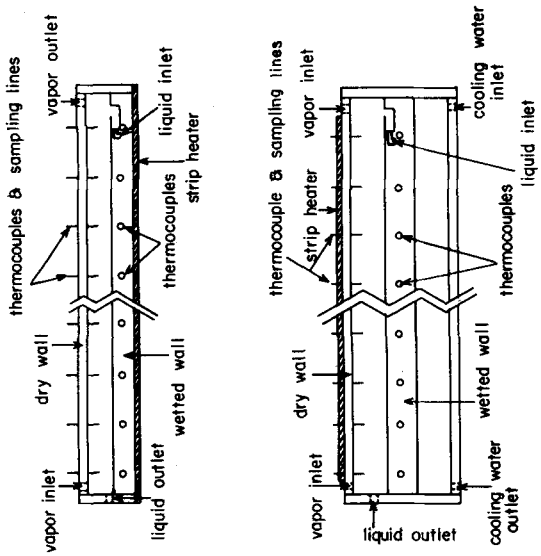

Figure 2. Single and double channel fractionators.

column was taken to be 1.8×10^{-5} kmol/s to 9.0×10^{-5} kmol/s.

Actually, two wetted-wall columns were constructed with identical channel cross-sections. A single-channel column was built for the evaporation experiments. Heat was supplied to the wetted-wall of this column by an 1,800 W strip heater. A dual-channel column was built for the condensation experiments. Heat was removed from the wetted-wall by cooling water which flowed downward in the adjacent channel. Schematics of these columns are shown in Figure 2.

In the dual-channel column, the cooling water was not only in contact with the wetted-wall but also with the side walls of the column. As a result there was a significant amount of heat transfer from the vapor phase to the cooling water by conduction through the side walls. To counteract this unwanted heat loss a 600 W strip heater was attached externally to the dry wall (opposite the wetted-wall) as shown in Figure 2. The amount of heat was adjusted to minimize the temperature difference between the vapor phase and the dry wall. The local temperature difference was determined from comparison of the vapor temperature measurements with the dry wall temperature measurements taken at three points spaced at 0.61 m intervals.

As shown in Figure 2, the dimensions of the liquid distributor dictated a rather thick wall through which heat was either added to or removed from the fractionation taking place in the flow channel. In order to reduce the complexity of the analysis of heat conduction in this wall, aluminum was chosen as the material of construction for these columns because of its large thermal conductivity. Over the operating range the temperature drop across the wall remained quite small and axial heat conduction effects were negligible (Davis and Gill 1970).

Each column was constructed from separate rectangular pieces of aluminum suitably bolted together. The particular aluminum alloy, 2024-T351 was chosen because of its superior machinability. Dow-Corning RTV-730, a fluorosilicone sealant, along with Dow-Corning binder #7, was used as the gasket. This material is highly resistant to both n-hexane and toluene over the expected operating temperature range and as a gasket aids in the reduction of heat transfer through the side walls. During operation the columns were insulated with a 10 cm layer of fiber glass insulation.

Even distribution of the liquid along the perimeter of the wall was accomplished with the usual distributor design in which the liquid spilled over a weir. Specifically, as shown in Fig. 2, the liquid flowed into a large circular channel from the side of the column. The liquid immediately spread across the width of the column in this channel from which it was next carried up into the open groove through a series of eleven holes. Two sections of wire mesh (not shown in Figure 2) were pressed into the groove to break up any

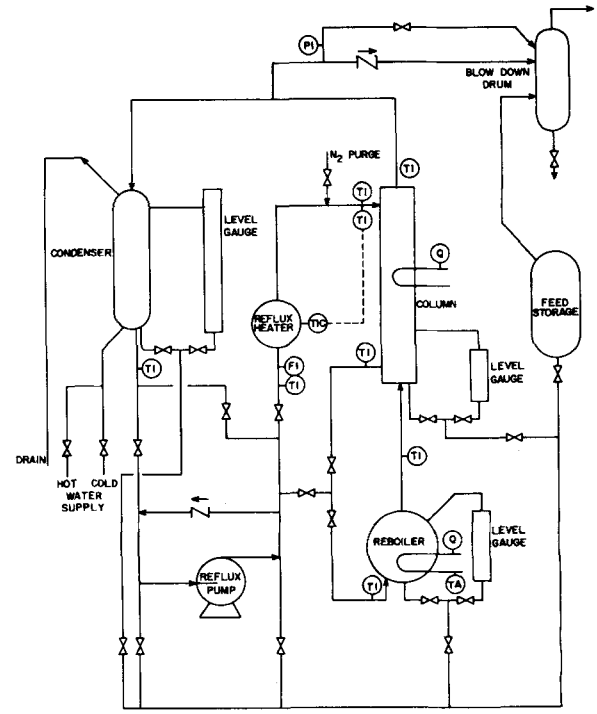

Figure 3. A flowsheet of the experimental unit.

vertical jets which might cause bumping in the overflowing liquid. The edge of the weir was machined into a very sharp knife edge. Thorough testing showed that this design was very effective for evenly distributing the liquid within the operating range of the column. However, even distribution was found to be very sensitive to any rotational misalignment of the distributor. To ensure an even distribution the column position was finely adjusted by means of a special mounting bracket.

Temperature and composition measurement points along the column length are shown also in Figure 2. As illustrated, at each of the eight positions vapor composition, vapor temperature, and wetted-wall temperature were measured. These measurement positions were spaced at 0.305 m intervals. Vapor temperature measurements were made using a Type T sheathed thermocouple which protruded 0.0032 m into the channel. Wall temperature measurements were made with Type T thermocouples inserted into a port drilled directly through the column side wall and into the wetted-wall. The depth of this port, 0.086 m, corresponds to the location of the vapor temperature and composition measurements on the dry wall. The precision of the temperature measurement system was determined to be ±0.05 K. A refractometer with a precision of ±0.002 mol fraction was used to analyze the vapor composition. Vapor samples were obtained by drawing small quantities of vapor off through 0.0032 m diameter tubing and then cooled to approximately 273 K before storing.

DESCRIPTION AND OPERATION OF THE EXPERIMENTAL UNIT

Figure 3 shows a schematic diagram for the experimental unit excluding the column heating or cooling systems. A kettle-type reboiler was used with heat supplied by two manually controlled 2,200 W immersion heaters. At full heating capacity the boil-up rate was approximately 1.3×10^{-4} kmol/s. A coil-type tube-and-shell heat exchanger was used for the condensation of the overhead vapor. The reflux was subcooled to prevent any vaporization in the reflux pump. Considerable flexibility in the cooling capacity was available by varying the cooling water flow rate and inlet temperature. Before entering the top of the column, the liquid reflux was brought back to the bubble point by means of a reflux heater,

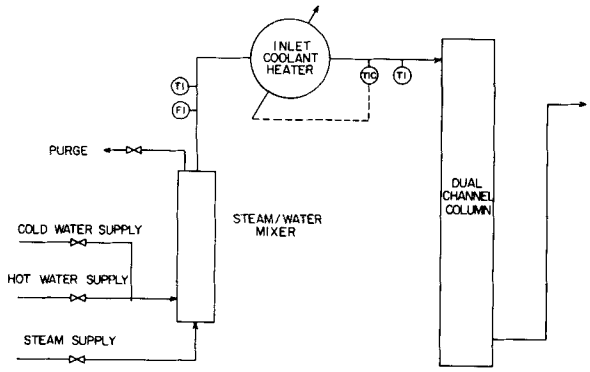

Figure 4. Coolant system used in fractionating condensation.

a long tube heated by a temperature-controlled, 800 W strip heater.

For the evaporation experiments in the single channel column heat was supplied to the wetted-wall by two manually controlled strip heaters each with a capacity of 900 W. However, a much more complex system was required to provide cooling water for the condensation experiments in the dual channel column. Figure 4 shows this cooling system. A steam-water mixer in which steam was supplied through a sintered metal sparge tube was used to obtain a water temperature which was maintained approximately at, but somewhat below, the desired inlet cooling water temperature. An automatic temperature-controlled heater was used for the final adjustments. To keep the cooling water flow rate at a minimum while maintaining well-mixed conditions, the coolant channel of the column was packed with 0.006 m glass beads.

The experimental unit was capable of operating very steadily for extended periods of time. This was true both for the evaporation and condensation experiments. Average steady-state fluctuations were ±350 Pa in the column pressure, $\pm 1.7 \times 10^{-7}$ m^3/s in the reflux flow rate, and ±0.5 K in the overhead vapor temperature. These values were based on a one hour time period during which three sets of measurements and samples were taken at half hour intervals.

Not a small concern in the design of the experimental unit was the high toxicity and flammability of the hexane-toluene mixture. With reference to Figure 3, a blow-down drum vented to the outside was used to catch any hydrocarbons escaping from the unit through relief or vent lines. A large portion of the process valving and piping was related to the nitrogen purge system. With this system, it was possible to sweep out any oxygen from all process lines and vessels prior to start up. At the end of a run all hydrocarbons were removed from the system for safe storage. Low heat flux heaters in the reboiler were used to avoid film boiling conditions, and a high temperature alarm would signal exposure of the immersion heaters resulting from a drop in the liquid level.

In addition to these measures, the unit was enclosed in a partial but well ventilated hood and was operated totally from outside the enclosure. Wiring inside the enclosure consisted only of electric heater connections. All relays, switches, controllers, and motors were located outside the enclosure. The heating wires of the strip heaters used inside the enclosure were sealed in vulcanized silicone rubber. Spills were doubly contained to prevent hydrocarbons from entering the building drain system. A dual sensor hydrocarbon detection system which monitors the enclosure would sound an alarm if the hydrocarbon level at either sensor reached 40% of the lower explosion limit.

COMPARISON OF RESULTS

Energy Balance Enclosures

Conditions for fractionating condensation and evaporation experiments are given in Table 2. The runs have been selected on the basis of energy balance closures around each column and to cover as wide a range of experimental conditions as possible.

The following terms enter into the energy balance around each column: vapor entering the bottom of the column from the reboiler, vapor leaving the top of the column, liquid reflux returning to the top of the column, liquid leaving the bottom of the column, heat input from the strip heater, heat removal by the cooling water, and heat losses to the surroundings.

Heat losses from the column and the reboiler are essentially accounted for by blank calibration runs. The reboiler vapor flow rate was calculated from an energy balance around the reboiler based on reboiler heat input and molar enthalpies of the vapor and

TABLE 2. OPERATION CONDITIONS FOR EVAPORATION AND CONDENSATION EXPERIMENTS

Run No.	Pres., atm	Reboiler Duty, W	Wall Heat Input, W	Composition Top	Composition Bot	Reflux Flow Rate kmol/s	Reboiler Vapor Flow Rate kmol/s Method A	Reboiler Vapor Flow Rate kmol/s Method B	Energy Closure Imbalance, W
					Evaporation Experiments				
3	1.019	1,230	0	0.924	0.693	4.001×10^{-5}	3.712×10^{-5}	3.697×10^{-5}	−32
4	1.019	1,230	293	0.920	0.698	5.002×10^{-5}	3.855×10^{-5}	3.702×10^{-5}	−53
7	1.019	1,230	0	0.883	0.633	3.932×10^{-5}	3.666×10^{-5}	3.581×10^{-5}	10
10	1.225	1,230	871	0.917	0.587	6.539×10^{-5}	3.629×10^{-5}	3.252×10^{-5}	87
11	1.226	1,230	1,259	0.948	0.590	8.442×10^{-5}	3.629×10^{-5}	3.911×10^{-5}	247
13	1.203	1,230	1,633	0.902	0.453	8.833×10^{-5}	3.541×10^{-5}	2.940×10^{-5}	130
14	1.325	1,230	1,179	0.869	0.381	7.144×10^{-5}	3.515×10^{-5}	2.668×10^{-5}	137
15	1.254	1,230	718	0.856	0.356	5.469×10^{-5}	3.503×10^{-5}	2.614×10^{-5}	259
16	1.260	1,230	1,633	0.873	0.361	8.303×10^{-5}	3.503×10^{-5}	2.324×10^{-5}	207
17	1.216	1,230	879	0.852	0.364	5.985×10^{-5}	3.503×10^{-5}	2.581×10^{-5}	198
					Condensation Experiments				
18	1.103	1,114	10	0.916	0.620	3.526×10^{-5}	3.438×10^{-5}	3.260×10^{-5}	−41
19	1.214	1,788	210	0.891	0.612	6.077×10^{-5}	5.282×10^{-5}	4.939×10^{-5}	−38
21	1.056	1,114	−400	0.928	0.587	2.272×10^{-5}	3.117×10^{-5}	3.427×10^{-5}	22
22	1.121	1,788	−540	0.902	0.568	4.169×10^{-5}	5.113×10^{-5}	4.659×10^{-5}	8
23	1.189	1,524	−223	0.870	0.542	3.268×10^{-5}	4.347×10^{-5}	3.389×10^{-5}	173
24	1.180	1,524	−530	0.886	0.536	2.535×10^{-5}	4.345×10^{-5}	4.055×10^{-5}	117
25	1.236	2,052	−540	0.869	0.520	4.579×10^{-5}	5.874×10^{-5}	5.979×10^{-5}	−25
26	1.235	2,052	−495	0.867	0.504	4.963×10^{-5}	5.858×10^{-5}	6.081×10^{-5}	−78
33	1.225	1,463	−728	0.875	0.545	2.731×10^{-5}	4.201×10^{-5}	4.064×10^{-5}	66
34	1.255	2,052	−153	0.869	0.531	5.661×10^{-5}	5.905×10^{-5}	5.637×10^{-5}	54
35	1.233	2,052	−640	0.861	0.498	3.886×10^{-5}	5.869×10^{-5}	5.564×10^{-5}	114
36	1.252	1,524	−197	0.857	0.397	3.698×10^{-5}	4.292×10^{-5}	3.899×10^{-5}	107
37	1.269	2,052	−703	0.838	0.362	3.713×10^{-5}	5.770×10^{-5}	5.204×10^{-5}	193
38	1.240	2,052	−322	0.830	0.323	4.361×10^{-5}	5.736×10^{-5}	4.869×10^{-5}	258

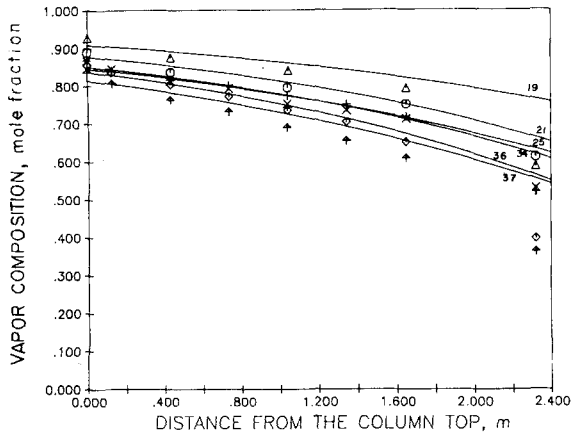

Run number	Experimental data	Run number	Experimental data
3		25	
4		34	
10		36	
13		37	
15		102	
16		105	
19		109	
21			

Figure 5. Vapor composition profiles in fractionating condensation.

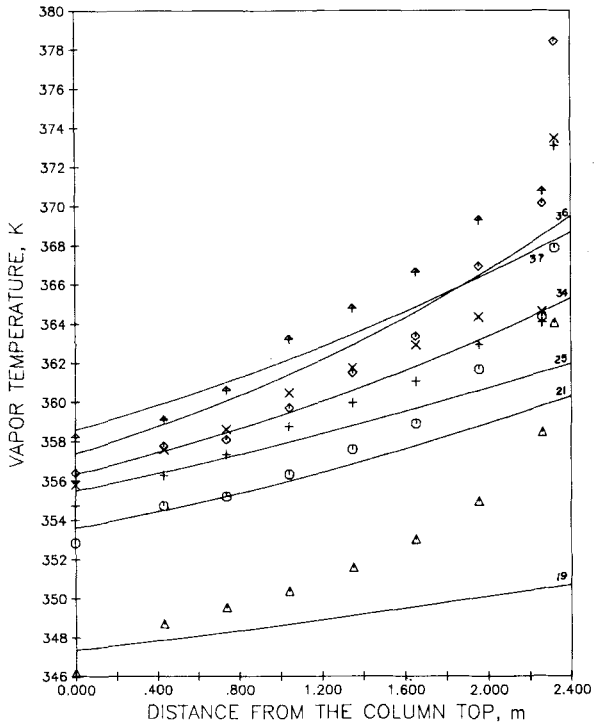

Figure 6. Vapor temperature profiles in fractionating condensation.

the liquid streams leaving the reboiler. The molar enthalpies were determined from vapor temperature, liquid temperature and liquid composition measurements. The reboiler heat input was determined from the calibration as described by Davis (1982).

Strip heaters were used for different purposes in the evaporation and condensation experiments. In the fractionating evaporation experiments, they were mounted on the wetted wall to provide the heat input Q which contributed to the evaporation. In order to account for heat losses, calibration experiments were carried out

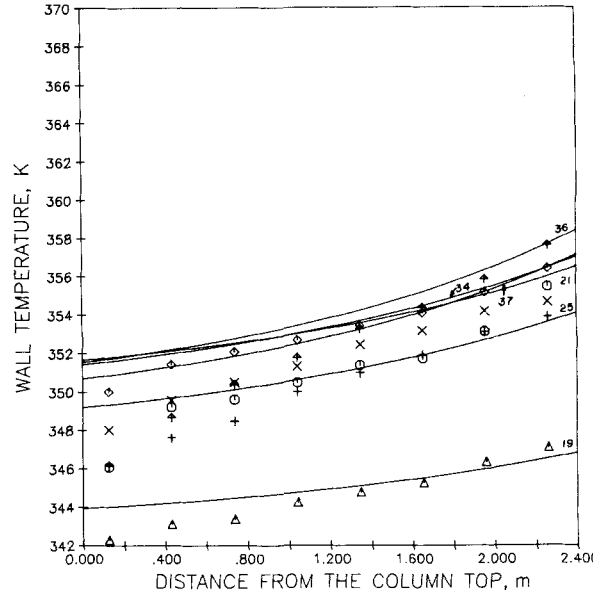

Figure 7. Wall temperature profiles in fractionating condensation.

to determine the heat input. In the fractionating condensation experiments, it was found that condensation was induced on the dry wall as a result of the cooling of the wetted wall. In order to eliminate this secondary effect strip heaters were mounted on the dry wall with the aim of maintaining the temperature of the dry wall at the same temperature as the local vapor temperature. In computing the wall heat flux in the condensation experiments, an assumption was made that the heat removal through the wetted wall was given by the difference between the overall enthalpy change of the cooling water and the overall heat input of the strip heaters. This assumption is reasonable, since the temperature differences between the dry wall and the vapor phase were observed to be less than 1.5 K.

Energy balance closures around each column are shown in the last column of Table 2. The maximum imbalance is 259 W or 13% of the total energy input into the column, and the average imbalance is 83 W or 4% of the total energy input into the column.

Temperature and Composition Profiles

As stated earlier, temperature and composition measurements along the length of the columns are desirable, because they allow the profiles to be compared more discriminantly with the experimental data with some allowance made for the entrance effects.

In our experiments it was found that the entrance effects were more pronounced for the vapor composition and vapor temperature near the bottom of the column and, in the condensation experiments, for the wall temperature near the top of the column. Fortunately, the wall temperature was not used directly in our computing procedure. It was possible to minimize the entrance effects in computation by starting the numerical integration from the top the column. Least-squares curve fitting of vapor temperature and vapor composition data by a second-order polynomial was used to yield "smoothed" initial conditions for numerical integration.

Figures 5–10 show the comparison of vapor composition, vapor temperature and wall temperature profiles. Runs 19, 21, 25, 34, 36 and 37 were chosen from the condensation experiments, while runs 3, 4, 10, 13, 15 and 16 were chosen from evaporation experiments.

For the vapor composition good agreement was obtained between the theoretical prediction and the experimental data with a maximum deviation of 0.03 mol fraction at $z = 1.6$ m, as shown in Figures 5 and 8. The bottom vapor composition was subject to large entrance effect and was not considered in this evaluation. In

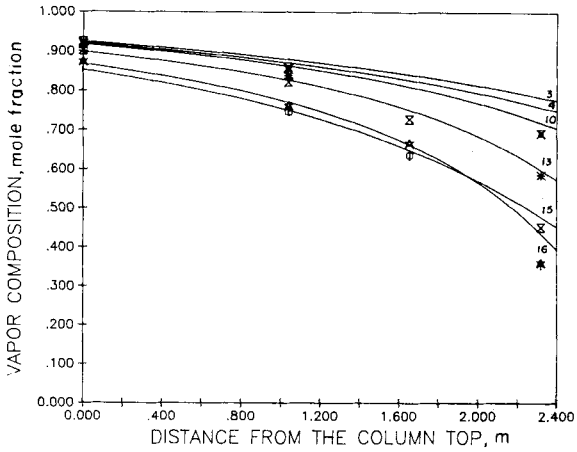

Figure 8. Vapor composition profiles in fractionating evaporation.

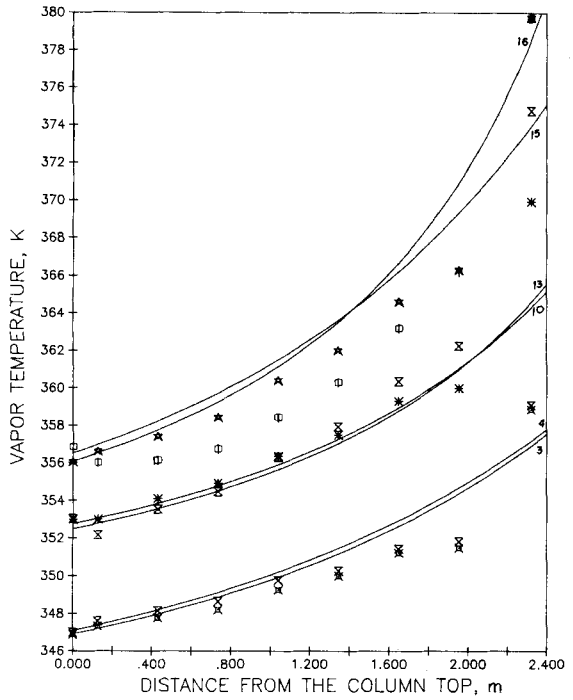

Figure 9. Vapor temperature profiles in fractionating evaporation.

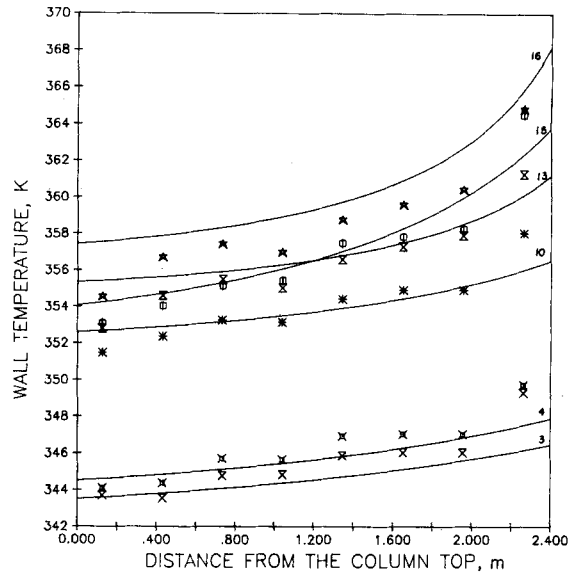

Figure 10. Wall temperature profiles in fractionating evaporation.

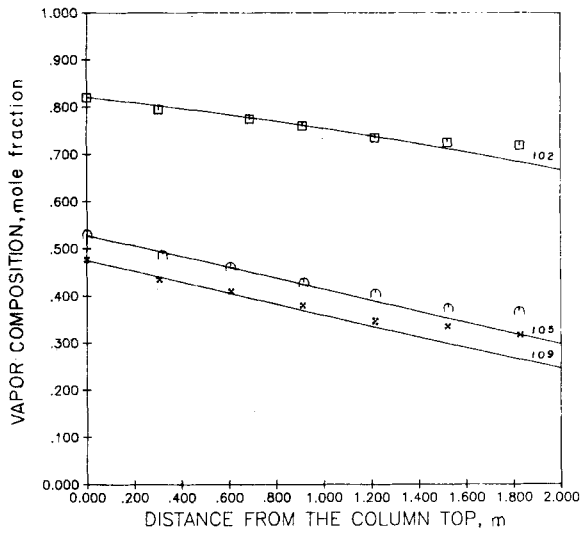

Figure 11. Vapor composition profiles based on Kent's data.

both evaporation and condensation experiments the model tends to slightly underpredict the variation of vapor composition along the column length. This could be caused by the deposition of liquid drops on the dry wall resulting in an increase of mass transfer area. Other potential contributing factors are the accuracy of vapor-phase mass transfer coefficient, the validity of the film theory, and the effect of liquid-phase mass transfer resistance. Precise evaluation of individual factors is not possible with the available experimental data.

Further validation of the model was made using vapor composition data reported by Kent (1953). Since values of vapor temperature and cooling water rate were not explicitly reported, we assumed that the mass flux through the vapor-liquid interface was uniform and that the vapor temperature at the top of the column was at its bubble point. The results plotted in Figure 11 show general agreement with the prediction.

The comparison of vapor temperature exhibits rather different trends. Figures 6 and 9 show that the model tends to underpredict the variation of vapor temperature in the condensation experiments with a maximum deviation of -6 K at $z = 1.6$ m, and overpredict its variation in the evaporation experiments with a maximum deviation of 4 K at $z = 1.6$ m. The deviation was probably caused by the approximation of the liquid temperature profile. For a finite wall heat input Q the model neglects any axial heat transfer due to the flow of the falling film. The net effect is to overestimate the heat addition to the vapor phase in evaporation and underestimate the heat removal from the vapor phase in condensation. Quantitatively, the 6 K deviation corresponds to a heat flow of less than 50 W, which is approximately 10% of the wall heat input for most of the experiments. Its impact is therefore less significant than it appears.

Wall temperature comparisons in Figures 7 and 10 also show good agreement. The best fit was obtained by using Eq. 11 to calculate the liquid-phase heat transfer coefficient for the condensation runs and Eq. 23 for the evaporation runs. Equation 23 which is based on the correlation of Chun and Seban (1973) is given below:

$$h_w = (4/3)^{1/3} \cdot (\rho_l^2 g k_l^3/\mu_l^2)^{1/3} Re_l^{-1/3} \quad \text{if } Re_l \le Re_l^*$$

$$h_w = 0.8221 \cdot (\rho_l^2 g k_l^3/\mu_l^2)^{1/3} Re_l^{-0.22} \quad \text{if } Re_l^* \le Re_l \le Re_l^{**} \tag{23}$$

where

$$Re_l = 4 \cdot |L| \cdot M_l/\mu_l, \quad Re_l^* = 2.44(\mu_l^4 g/\rho_l \sigma^3)^{-1/11},$$
$$Re_l^{**} = 5{,}800\, Pr_l^{-1.06}$$

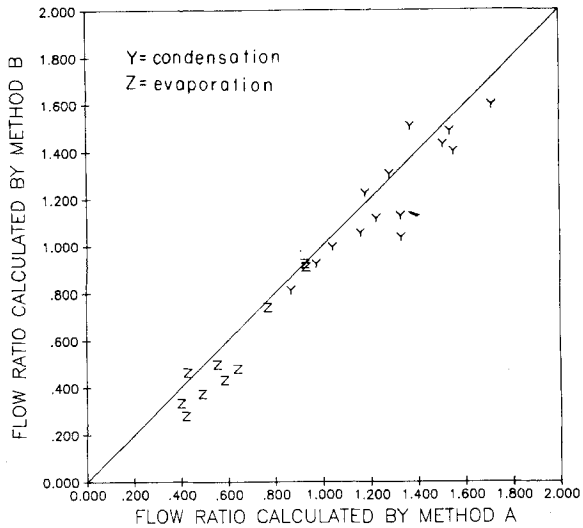

Figure 12. The ratios of reboiler vapor flow rate to reflux flow rate as calculated using method A & B.

Equation 23 which is applicable to the evaporating conditions generally predicts a heat transfer coefficient 40% higher than Eq. 11 which is derived on the basis of laminar flow. It is known from linear stability analysis that evaporation destabilizes the surface waves (Bankoff, 1971) and condensation stabilizes surface waves (Marshall et al., 1973). Since surface waves were probably present in our experiments, they provide an explanation why the two different equations, Eqs. 23 and 11, appear to apply to the evaporation and condensation data, respectively.

For runs 19, 34 and 36 the imbalance in energy balance closure is of the same order of magnitude as the maximum wall heat input (210 W), and wall temperature deviations of 1–2 K were observed. These deviations disappeared at higher wall heat input.

Reboiler Vapor Flow Rate

Another important check on the model is its prediction of vapor flow rate along the length of the column. Direct measurements on this variable were not available in our experiments. However, as discussed earlier, we did have an indirect estimate of the reboiler vapor flow rate which would be, in general, affected by the entrance effects. Vapor flow rates estimated by this method are listed in Table 2 under Method A. Corresponding values obtained from numerical integration are listed in the same table under Method B.

Comparison shows that the maximum deviation is only 1.2×10^{-5} kmol/s. The ratio r of reboiler vapor flow rate to reflux flow rate is a measure of the variation of flow rates along the length of the column. Values of this ratio obtained by these two methods are plotted against each other in Figure 12. The results agree to within 10%.

CLOSING REMARKS

In this study a model was proposed for predicting the behavior of falling film fractionators under nonadiabatic operating conditions. Linear transveral temperature profile and zero mass transfer resistance were assumed for the liquid phase. The broad agreement between the prediction and the experimental data suggests that the model is basically correct.

Experimental results of Kent and Pigford (1956) and of Onda et al. (1970) indicated that mass transfer resistance in the liquid phase, though small, could still be significant. This suggests that the proposed model might be improved, if the above assumptions were relaxed. The model was modified by assuming that in the liquid phase there exists a thin region adjacent to the vapor-liquid interface where simultaneous heat and mass transfer occur. Similarly, it was assumed that there is another thin region adjacent to the wetted wall where heat transfer between the wall and the liquid takes place. This model was generally plagued by numerical difficulties. For the case for which comparison was possible agreement between predictions and experimental data was poor (Davis, 1982). The numerical instabilities and inaccuracies were attributed to the extremely small temperature and composition differences in the liquid phase encountered in the computation.

The proposed model is simple to compute and numerically stable. It gives predictions with an accuracy warranted by the quality of the currently available experimental data.

ACKNOWLEDGMENT

This work was supported by the National Science Foundation Grant CPE-8120564.

NOTATION

a = wetted area per unit volume, 1/m
Cp = heat capacity, J/kg·K
d = hydraulic diameter defined as four × cross-sectional area/perimeter, m
$\mathcal{D}_{12}$ = mass diffusivity, m^2/s
g = gravitational acceleration, m/s^2
$\mathcal{H}$ = vapor molar enthalpy, J/kmol
H_G = vapor film heat transfer coefficient, $W/m^2 \cdot K$
$\mathcal{h}$ = liquid molar enthalpy, J/kmol
h = liquid heat transfer coefficient, $W/m^2 \cdot K$
k = thermal conductivity, W/m·K
K_G = vapor mass transfer coefficient, kmol/s·m^2
L = liquid molar flow rate per wetted perimeter, kmol/s·m
M = molecular weight, kg/kmol
N = interfacial molar flux, kmol/s·m^2
P = reference pressure, Pa
p = pressure, Pa
Pr = Prandtl number, $\mu Cp/k$
Q = wall heat input per unit area of the wall, W
Re = Reynolds number, $W \cdot d \cdot M_v/\mu_v$ or $4|L| \cdot M_l/\mu_l$
r = ratio of reboiler vapor flow rate to reflux flow rate
S = characteristic length in the s direction, m
s = coordinate in the horizontal direction
Sc = Schmidt number, $\mu/\rho\mathcal{D}_{12}$
T = vapor temperature, K
t = liquid temperature, K
U = characteristic velocity, m/s
u = liquid velocity, m/s
V = vapor molar flow rate per wetted perimeter, kmol/s·m
W = vapor molar flux, kmol/s·m^2
x,y = mole fraction or mass fration of the more volatile component in liquid and vapor phases
Z = characteristic length in the z direction, m
z = coordinate in the vertical direction

Greek Letters

δ = film thickness, m
ϵ = small parameter
λ = latent heat, J/kmol
μ = viscosity, kg/m·s
ν = kinematic viscosity, m^2/s
ρ = density, kg/m^3
σ = surface tension, N/m

Subscripts

1 = component one, more volatile component
2 = component two, less volatile component

i = interface
l = liquid
s = s direction
w = wall
v = vapor
z = z direction

Superscripts

• = corrected transfer coefficient
′ = dimensionless term

APPENDIX: DERIVATION OF LIQUID-PHASE TRANSPORT EQUATIONS

If we assume that

1. The liquid physical properties are constant.
2. The heat conduction and mass diffusion in the z direction are negligible.
3. The term containing $\partial^2 x/\partial s^2$ is negligible in the energy balance.

then the equations of continuity, momentum and energy in the liquid film can be expressed in rectangular coordinates as follows:

$$\frac{\partial u_z}{\partial z} + \frac{\partial u_s}{\partial s} = 0 \tag{A1}$$

$$u_z \frac{\partial u_z}{\partial z} + u_s \frac{\partial u_z}{\partial s} = \frac{\mu_l}{\rho_l}\frac{\partial^2 u_z}{\partial s^2} - g - \frac{1}{\rho_l}\frac{\partial p}{\partial z} \tag{A2}$$

$$u_z \frac{\partial t}{\partial z} + u_s \frac{\partial t}{\partial s} = \frac{k_l}{\rho_l Cp_l}\frac{\partial^2 t}{\partial s^2} + \frac{\mathcal{D}_{12,l}}{Cp_l}(Cp_{l,1} - Cp_{l,2})\frac{\partial t}{\partial s}\frac{\partial x}{\partial s} \tag{A3}$$

where u_z and u_s are liquid velocities in z and s directions, respectively. p is the pressure, t is the temperature, k_l is thermal conductivity, Cp_l is the heat capacity, ρ_l is density, $\mathcal{D}_{12,l}$ is mass diffusivity coefficient and x is the mass fraction all with reference to the liquid.

Similarly, the component mass balance can be written as:

$$u_z \frac{\partial x}{\partial z} + u_s \frac{\partial x}{\partial s} = \mathcal{D}_{12,l}\frac{\partial^2 x}{\partial s^2} \tag{A4}$$

These equations may be rendered dimensionless by replacing the variables by their dimensionless counterparts as follows:

$$\frac{\partial u_z'}{\partial z'} + \frac{ZU_s}{SU_z}\frac{\partial u_s'}{\partial s'} = 0 \tag{A5}$$

$$u_z'\frac{\partial u_z'}{\partial z'} + \frac{ZU_s}{SU_z}u_s'\frac{\partial u_z'}{\partial s'} = \frac{ZU_s}{SU_z}\frac{\nu_l}{U_s S}\frac{\partial^2 u_z'}{\partial s'^2} - \frac{gZ}{U_z^2} - \frac{P}{\rho_l U_z^2}\frac{\partial p'}{\partial z'} \tag{A6}$$

$$u_z'\frac{\partial t'}{\partial z'} + \frac{ZU_s}{SU_z}u_s'\frac{\partial t'}{\partial s'} = \frac{1}{Pr_l}\frac{\nu_l}{U_s S}\frac{ZU_s}{SU_z}\frac{\partial^2 t'}{\partial s'^2} + \frac{Cp_l'}{Sc_l}\frac{\nu_l}{U_s S}\frac{\partial t'}{\partial s'}\frac{\partial x}{\partial s'} \tag{A7}$$

$$u_z'\frac{\partial x}{\partial z'} + \frac{ZU_s}{SU_z}u_s'\frac{\partial x}{\partial s'} = \frac{1}{Sc_l}\frac{\nu_l}{U_s S}\frac{ZU_s}{SU_z}\frac{\partial^2 x}{\partial s'^2} \tag{A8}$$

where ν_l is liquid kinematic viscosity, $Cp_l' = (Cp_{l,1} - Cp_{l,2})/Cp_l$, $Pr_l = \mu_l Cp_l/k_l$ and $Sc_l = \mu_l/\rho_l \mathcal{D}_{12,l}$ and

$$z' = z/Z; \quad s' = s/S; \quad u_z' = u_z/U_z; \quad u_s' = u_s/U_s;$$
$$p' = p/P; \quad t' = (t - t_w)/(t_i - t_w).$$

P is the reference pressure, and S, Z, U_z and U_s are the characteristic lengths and velocities in the s and z directions, respectively.

Let ϵ denote the Reynolds number based upon s direction flow, $U_s S/\nu_l$, and let us assume that $\epsilon \ll 1$. Applying the boundary layer approximation $ZU_s/SU_z = 1$, we obtain from Eqs. A6–A8,

$$u_z'\frac{\partial u_z'}{\partial z'} + u_s'\frac{\partial u_{z'}}{\partial s'} = \frac{1}{\epsilon}\frac{\partial^2 u_z'}{\partial s'^2} - \frac{gZ}{U_z^2} - \frac{P}{\rho_l U_z^2}\frac{\partial p'}{\partial z'} \tag{A9}$$

$$u_z'\frac{\partial t'}{\partial z'} + u_s'\frac{\partial t'}{\partial s'} = \frac{1}{Pr_l}\frac{1}{\epsilon}\frac{\partial^2 t'}{\partial s'^2} + \frac{Cp_l'}{Sc_l'}\frac{1}{\epsilon}\frac{\partial t'}{\partial s'}\frac{\partial x}{\partial s'} \tag{A10}$$

$$u_z'\frac{\partial x}{\partial z'} + u_s'\frac{\partial x}{\partial s'} = \frac{1}{Sc_l}\frac{1}{\epsilon}\frac{\partial^2 x}{\partial s'^2} \tag{A11}$$

Neglecting the terms $O(\epsilon)$, we obtain the zero-order approximations as follows:

$$\frac{\partial^2 u_z'}{\partial s'^2} = \epsilon\frac{gZ}{U_z^2} \tag{A12}$$

$$\frac{1}{Pr_l}\frac{\partial^2 t'}{\partial s'^2} = -\frac{Cp_l'}{Sc_l}\frac{\partial t'}{\partial s'}\frac{\partial x}{\partial s'} \tag{A13}$$

$$\frac{\partial^2 x}{\partial s'^2} = 0 \tag{A14}$$

The gravity term is retained because the flow is gravity-driven in our case.

To render them comparable to Eqs. 7–9, these equations can be rewritten in dimensional form as:

$$\mu_l\frac{\partial^2 u_z}{\partial s^2} = \rho_l g \tag{A15}$$

$$\frac{\partial^2 t}{\partial s^2} = -\frac{Pr_l}{Sc_l}\cdot Cp_l'\frac{\partial t}{\partial s}\frac{\partial x}{\partial s} \tag{A16}$$

$$\frac{\partial^2 x}{\partial s^2} = 0 \tag{A17}$$

Integrating with the boundary conditions,

$$\left.\begin{aligned} u_z &= 0 \\ -k_l\frac{\partial t}{\partial s} &= Q \\ \frac{\partial x}{\partial s} &= 0 \end{aligned}\right\} \text{ at } S = 0 \tag{A18, A19, A20}$$

and

$$\left.\begin{aligned} \frac{\partial u_z}{\partial s} &= 0 \\ t &= t_i \\ x &= x_i \end{aligned}\right\} \text{ at } s = \delta_l \tag{A21, A22, A23}$$

we obtain Eqs. 7–9. Equation 7 is clearly valid in terms of mass fractions also.

LITERATURE CITED

Bankoff, S. G., "Stability of Liquid Flow down a Heated Inclined Plane," *Int. J. Heat Mass Transfer*, **14**, p. 377 (1971).

Bergles, A. E., J. G. Collier, J. M. Delhaye, G. H. Hewitt, and F. Mayinger, *Two-Phase Flow and Heat Transfer in the Power and Process Industries*, Ch. 18, "Multicomponent Boiling and Condensation," Hemisphere Publishing Corp. (1981).

Bird, R. B., W. E. Stewart, and E. N. Lightfoot, *Transport Phenomena*, p. 658 (1960).

Chilton, T. H., and A. P. Colburn, "Mass Transfer (Absorption) Coefficients," *Ind. Eng. Chem.*, **26**, p. 1183 (1934).

Chun, K. R., and R. A. Seban, "Performance Prediction of Falling-Film Evaporators," *Trans. ASME, J. Heat Transfer*, p. 432 (Nov., 1973).

Clift, R., C. L. Pritchard, and R. M. Nedderman, "The Effect of Viscosity on the Flooding Conditions in Wetted Wall Columns," *Chem. Eng. Sci.*, **21**, p. 87 (1966).

Colburn, A. P., and T. B. Drew, "The Condensation of Mixed Vapors," *Trans. AIChE*, **33**, p. 197 (1937).

Davis, E. J., and W. N. Gill, "The Effects of Axial Conduction in a Wall on Heat Transfer with Laminar Flow," *Int. J. Heat Mass Transfer*, **13**, p. 459 (1970).

Davis, J. F., "Distillation with Secondary Reflux and Vaporization: Simultaneous Heat and Mass Transfer in a Wetted Wall Fractionating Evaporator," Ph.D. Thesis, Northwestern University (1982).
Denny, V. E., and V. J. Jusionis, "Effects of Forced Flow and Variable Properties on Binary Film Condensation," *Int. J. Heat Mass Transfer*, **15**, p. 2143 (1972).
Feintuch, H. M., and R. E. Treybal, "The Design of Adiabatic Packed Towers for Gas Adsorption and Stripping," *Ind. Eng. Chem. Process Des. Dev.*, **17**, p. 505 (1978).
Fitzmorris, R. E., and R. S. H. Mah, "Improving Distillation Column Design Using Thermodynamic Availability Analysis," *AIChE J.*, **26**, p. 265 (1980).
Harnett, J. P., J. C. Y. Koh, and S. T. McComas, "A Comparison of Predicted and Measured Frictions for Turbulent Flow through Rectangular Ducts," *Trans. ASME, J. Heat Transfer*, **84**, p. 82 (1962).
Hewitt, G. F., and N. S. Hall-Taylor, *Annular Two Phase Flow*, Pergamon Press (1970).
Hirata, M., S. Ohe, and K. Nagahama, *Computer Aided Data Book of Vapor-Liquid Equilibria*, Elsevier, New York (1975)
Hoffman, E. J., "Partial Condensation by Methods of Simulataneous Heat and Mass Transfer," *AIChE J.*, **17**, p. 741 (1971).
Ito, A., and K. Asano, "Thermal Effects in Non-adiabatic Binary Distillation," *Chem. Engng. Sci.*, **37**, p. 1007 (1982).
Kent, E. R., "Mass Transfer in a Wetted Wall Column with Emphasis on Partial Condensation," Ph.D. Thesis, University of Delaware (1953).
Kent, E. R., and R. L. Pigford, "Fractionation During Condensation of Vapor Mixtures," *AIChE J.*, **2**, p. 363 (1956).
Krishna, R., "Binary and Multicomponent Mass Transfer at High Transfer Rate," *Chem. Eng. J.*, **20**, p. 251 (1981).
Krishna, R., and C. B. Panchal, "Condensation of a Binary Vapor Mixture in the Presence of an Inert Gas," *Chem. Eng. Sci.*, **32**, p. 741 (1977).
Kotake, S., and K. Oswatitsch, "Parameters of Binary-Mixture Film Condensation," *Int. J. Heat Mass Transfer*, **23**, p. 1405 (1980).
Mah, R. S. H., "Performance Evaluation of Distillation Systems," *Foundations of Computer-Aided Chemical Process Design*, R. S. H. Mah and W. D. Seider, Eds., Engineering Foundation and AIChE (1981).
Mah, R. S. H., J. J. Nicholas, Jr., and R. B. Wodnik, "Distillation with Secondary Reflux and Vaporization: A Comparative Evaluation," *AIChE J.*, **23**, p. 651 (1977).
Marshall, E., and C. Y. Lee, "Stability of Condensate Flow down a Vertical Wall," *Int. J. Heat Mass Transfer*, **16**, p. 41 (1973).
Onda, K., E. Sada, and K. Yakahashi, "The Film Condensation of Mixed Vapor in a Vertical Column," *Int. J. Heat Mass Transfer*, **13**, p. 1415 (1970).
Perry, R. H., and C. H. Chilton, Eds., *Chemical Engineer's Handbook*, 5th Ed., McGraw Hill Book Co. (1973).
Ponter, A. B., G. A. Davis, T. K. Ross, and P. G. Thornley, "The Influence of Mass Transfer of Liquid Film Breakdown," *Int. J. Heat Mass Transfer*, **10**, p. 349 (1967).
Pratt, H. C., and P. G. Tuohey, "Binary and Multicomponent Mass Transfer at High Transfer Rates," *Chem. Eng. J.*, **18**, p. 251 (1979).
Price, B. C., and K. J. Bell, "Design of Binary Vapor Condensers Using the Colburn Drew Equations," *AIChE Symp. Ser.*, **70**, p. 163 (1974).
Reid, R. C., J. N. Prausnitz, and T. K. Sherwood, *The Properties of Gases and Liquids: Their Estimation and Correlation*, McGraw-Hill Book Co. (1977).
Schrodt, J. T., "Simultaneous Heat and Mass Transfer from Multicomponent Condensing Vapor-Gas System," *AIChE J.*, **19**, p. 753 (1973).
Stocker, U. V., and C. R. Wilke, "Rigorous and Short-Cut Design Calculations for Gas Absorption Involving Large Heat Effects. 1. A New Computational Method for Packed Gas Absorbers," *Ind. Eng. Chem. Fund.*, **16**, p. 88 (1977a).
——, "Rigorous and Short-Cut Design Calculations for Gas Absorption Involving Large Heat Effects. 2: Rapid Short-Cut Design Procedure for Packed Gas Absorbers," *ibid.*, **16**, p. 94 (1977b).
Shock, R. A. W., "Evaporation of Binary Mixtures in Upward Annular Flow," *Int. J. Multiphase Flow*, **2**, p. 411 (1976).
Sparrow, E. M., and E. Marshall, "Binary Gravity-Flow Film Condensation," *J. Heat Transfer*, **91**, p. 205 (1969).
Treybal, R. E., "Adiabatic Gas Absorption and Stripping in Packed Towers," *Ind. Eng. Chem.*, **61**, p. 36 (1969).
Van Es, J. P., and P. M. Heertjes, "The Condensation of a Vapor of a Binary Mixture," *Brit. Chem. Eng.*, **7**, p. 580 (1962).
Watanabe, K., and T. Munakata, "Distillation Performance of Externally Heated or Cooled Differential Contacting Column," *J. Chem. Eng. of Japan*, **9**, p. 113 (1976).

Manuscript received January 28, 1983; revision received May 11, and accepted May 19, 1983.

R & D NOTES

Wall Shear Measurements by Electrochemical Probe for Gas-Liquid Two-Phase Flow in Vertical Duct

G. COGNET, M. LEBOUCHE, and M. SOUHAR

Institut National Polytechnique de Lorraine
Nancy, France

For over 40 years, gas-liquid two-phase flows have been very important in the field of industrial sciences as their heat and mass transfer properties, particularly in chemical, oil and nuclear engineering.

These flows are usually classified according to the relative configuration of the two phases, mainly by geometrical and visual criteria (buble, slug, annular flows, etc.).

To better understand the transport phenomena in these rather complicated flows, we need more experimental data, among which is the momentum transferred to the wall by the shear stress. Usually this quantity is indirectly obtained from overall measurements (total pressure drop, average void fraction, etc.). In vertical ducts, the pressure loss by friction is small compared with the total pressure drop and the pressure loss by gravity (weight of the fluid column); therefore, a small error concerning these two terms may involve a considerable uncertainty for the friction. This leads to the interest on the direct measurement of the local wall shear stress.

The electrochemical technique using probes mounted flush to the wall appeared to be convenient for that purpose.

TECHNIQUE OF MEASUREMENT AND EXPERIMENTAL CONDITIONS

In the electrochemical method called "Polarography," the electrolysis current, I, which results from the transfer of active ions to the electrode, is controlled by hydrodynamic conditions (Reiss and Hanratty, 1962; Lebouché and Cognet, 1967; Mizushina, 1971).